Int. Journal of Refractory Metals & Hard Materials 27 (2009) 282–287

Contents lists available at ScienceDirect

Int. Journal of Refractory Metals & Hard Materials

journal homepage: www.elsevier.com/locate/IJRMHM

Measurement of residual thermal stress in WC–Co by neutron diffraction

D. Mari [a,*], B. Clausen [b], M.A.M. Bourke [b], K. Buss [a]

[a] Ecole Polytechnique Fédérale de Lausanne (EPFL), Institut de Physique de la Matière Complexe, CH-1015 Lausanne, Switzerland
[b] Los Alamos National Laboratory, New Mexico 87545, USA

ARTICLE INFO

Article history:
Received 12 September 2008
Accepted 27 November 2008

Keywords:
Cemented carbides
Cobalt
WC
Residual stresses
Thermal expansion

ABSTRACT

The temperature dependence of residual stresses in a WC–17.8vol.%Co cemented carbide was measured by neutron diffraction. The comparison of the WC lattice parameter within the WC–Co and within stress-free WC reference provides a measurement of lattice elastic strains and, using Hooke's law, stresses. WC is found to be under hydrostatic compressive stresses of about −400 MPa at room temperature, which decrease monotonically with temperature to a near-zero value at 800 °C. Residual stresses in cobalt also decrease with increasing temperature, but show an apparent increase above 800 °C, which is attributed to an increase in lattice parameter due to W dissolution in the Co phase.

© 2008 Elsevier Ltd. All rights reserved.

1. Introduction

WC–Co cemented carbides are materials widely used for the manufacturing of cutting tools. They are known for their exceptional combination of toughness and hardness. However, severe cutting conditions implying high temperature and stress produce plastic deformation of the cutting tool tips. Therefore, a better knowledge of the material behaviour at high temperature is needed to improve the quality of the tools. The stress field influencing the microstructure not only derives from the applied load but also from internal stress. As thermal expansion coefficients between WC and Co differ by a factor of three, cooling from the sintering temperature of about 1400 °C to lower temperatures can produce extremely high residual stresses. Measurement of residual strains (stresses) in composites is obtained from the comparison of in situ measured lattice parameters for each phase with a stress-free reference. Diffraction measurements of residual thermal stresses have been performed by different authors [1–6] both by X-rays and neutrons. The high tungsten content considerably limits the penetration depth of X-rays and measurements are sensitive to polishing and annealing. Hence, neutrons are a better choice to measure bulk properties of WC–Co. On the other hand, in WC–Co, due to the high elastic modulus of WC, a very good precision in measurements is required to obtain elastic strains with adequate accuracy. In order to reduce experimental errors in neutron diffraction measurements, differences in positioning and temperature between reference sample and the composite material must be minimum. At room temperature, compressive residual stresses around −500 MPa in WC and tensile stresses around 2000 MPa for cobalt are expected in a WC-18vol.%Co [4]. As temperature is increased, thermal stresses are expected to relax. A curious behaviour was found by [4] where thermal stresses started to increase again by heating above 800 °C. A thermal hysteresis between heating and cooling cycle was also observed. Since strains of the WC lattice are extremely small, it is not clear whether such behaviour should have been attributed to some experimental error. The purpose of this work is to measure the residual stress in both phases of a WC-17.8vol.%Co with high accuracy. We use a particular setup and time-of-flight neutron diffraction in order to achieve maximum precision and temperature reproducibility in the measurements of the composite materials and of the WC and Co references. The changes of residual stresses in the WC and Co phases are measured up to 1156 °C.

2. Materials and experimental methods

WC–Co samples with 17.8vol.% cobalt were prepared by AB Sandvik Coromant (Stockholm, Sweden). This high cobalt grade allows the measurement of both WC and Co diffraction peaks with good intensity. Bars of $89 \times 19 \times 4.5\ mm^3$ were produced by a usual sintering process. The SEM micrograph in Fig. 1 shows the general grain morphology. The average WC grain size is 1.8 μm.

Neutron diffraction measurements were performed in "time-of-flight" mode using the SMARTS diffraction instrument [7] at the pulsed neutron source at the Lujan Center of the Los Alamos National Laboratory (NM, USA). Detector banks positioned at ±90° angle with respect to the incident beam collect a complete diffraction

* Corresponding author. Tel.: +41 21 693 4473; fax: +41 21 693 4470.
E-mail address: daniele.mari@epfl.ch (D. Mari).

0263-4368/$ - see front matter © 2008 Elsevier Ltd. All rights reserved.
doi:10.1016/j.ijrmhm.2008.11.015

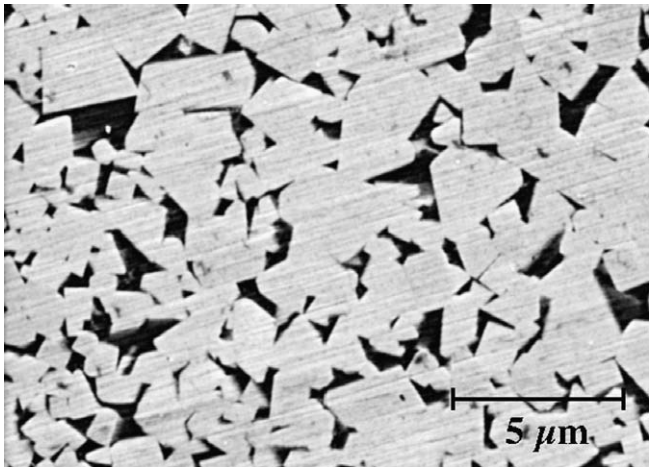

Fig. 1. SEM micrograph of the WC–Co morphology. WC grains are brighter.

pattern from neutrons having a white spectrum produced from a spallation source (Fig. 2a). Diffraction spectra with a d-spacing range between 0.2 and 3 Å are gathered simultaneously for the two banks. The spectra are analysed using the Rietveld refinement method using the GSAS software [8].

We used a particular sample geometry and the possibility offered by SMARTS to translate the specimens inside the furnace (Fig. 2b). Bulk sintered WC–Co samples were spark machined in order to make two windows at an angle of 45° with respect to the specimen axis to host the WC and the Co references. A slit was used to collimate the beam in the area of interest. With such geometry, the diffracted beam crosses always the same amount of material within the WC–Co support.

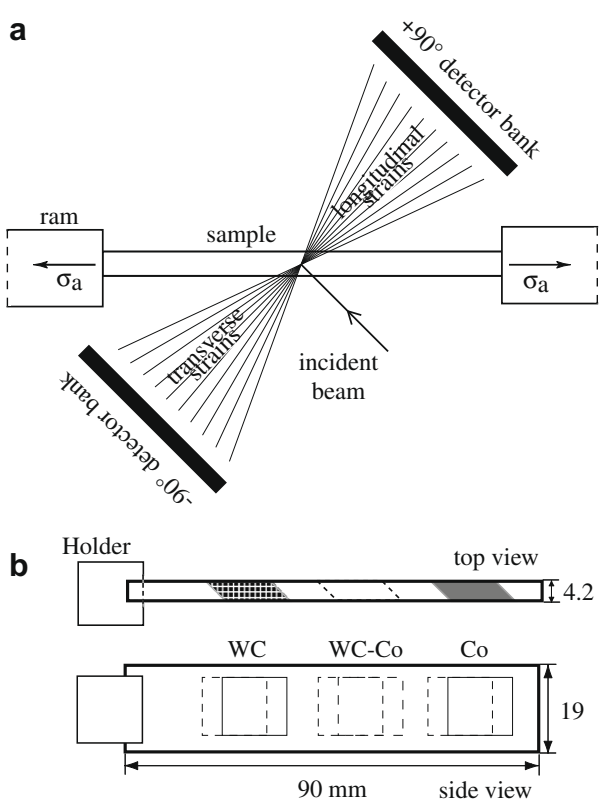

Fig. 2. (a) Schematic diagram of neutron diffraction. The SMARTS system is designed for diffraction under applied load. Crystal planes perpendicular to load axis diffract on the −90° detector bank while those parallel diffract on the opposite direction (b) drawing of the WC–Co frame and windows. In the present experiment, we use the load ram to shift the sample and to expose to radiation different windows in the WC–Co frame. In the WC–Co region, there is no window and the diffracting material is the frame itself. Two independent spectra are collected on both diffraction banks.

In a first experiment, not presented here, we noticed that the use WC powder as a reference may affect the measurement of the lattice parameter due to beam attenuation and consequent shift of the diffraction center of the specimen. In order to obtain a WC reference with a density equal to that found in sintered WC–Co, we etched the cobalt with boiling HCl from WC–Co and inserted the remaining WC 'skeleton' in the WC–Co frame as shown in Fig. 2. A stress-free reference for the cobalt cannot be produced, since in WC–Co, cobalt makes a solid solution with tungsten and carbon with a composition that varies with temperature [4]. Therefore, we used commercially pure cobalt made of 0.5 mm sheets forming a stack inserted in the cobalt reference window.

The sample assembly is mounted inside a vacuum furnace. The temperature of the furnace is controlled by two thermocouples positioned between the measurement windows. The temperature stability recorded during the measurements was better than ±1 °C.

The thermal strains in the WC phase are determined for the two lattice parameters a and c of the hexagonal WC lattice with respect to the lattice parameters a_0 and c_0 of the stress-free WC skeleton sample according to equations:

$$\varepsilon_a = \frac{a - a_0}{a_0} \quad \varepsilon_c = \frac{c - c_0}{c_0} \tag{1}$$

Subtracting the reference sample parameters is necessary to offset thermal expansion. Stresses are calculated using WC single crystal elastic constants [9] and the model of Evenschor et al. [10] to calculate stress in the Reuss limit (homogeneous stress) for hexagonal crystals. The following equations are used to convert strain ε to stress σ for the hexagonal axes a and c [4]:

$$\begin{aligned} \sigma_a &= 946\varepsilon_a + 259\varepsilon_c \ [\text{GPa}] \\ \sigma_c &= 627\varepsilon_a + 998\varepsilon_c \ [\text{GPa}] \end{aligned} \tag{2}$$

The mean hydrostatic stress σ_h in WC can then be calculated according to:

$$\sigma_{WC,h} = \frac{2\sigma_a + \sigma_c}{3} \tag{3}$$

The cobalt has an fcc structure in WC–Co and in our calculations we assume that it is elastically isotropic. The lattice strains in the Co phase result from the sum of mechanical strain in the composite and change in chemical composition of the alloy. In particular, the effect of W and C solid solution on cobalt lattice parameter has been studied by several authors [11–13].

Therefore we can write:

$$\varepsilon_{Co,tot} = \varepsilon_{Co,mech} + \varepsilon_{Co,chem} \tag{4}$$

The mechanical strain should obey the force balance relation:

$$f\sigma_{Co,mech} + (1 - f)\sigma_{WC,h} = 0 \tag{5}$$

where f is the volume fraction of the Co phase.

3. Results

3.1. Measurement of residual thermal stresses

Two heating-cooling cycles up to 1156 °C were performed. Since the differences between the data collected in the two cycles are small and within the measurement error, the figures presented below correspond to data collected in first cooling and second heating.

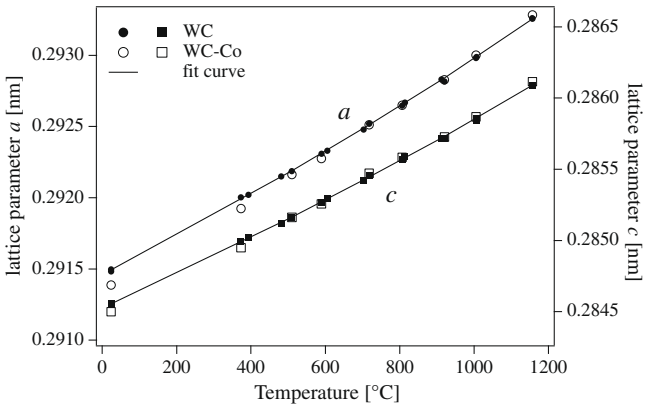

Fig. 3. Temperature dependence of WC lattice parameters *a* and *c* measured in WC skeleton (heating and cooling) and in WC–Co (heating). Thermal expansion of pure WC is shown in fitted curves. Polynomial fit coefficients are reported in Table 1.

In Fig. 3, the thermal expansion of WC measured in the WC skeleton is shown for both hexagonal principal axis *a* and *c*. The polynomial fit of thermal expansion, shown as a continuous line, is given in Table 1. It is in reasonable agreement with the data of thermal expansion of WC given by [14]. The WC lattice parameters obtained in WC–Co lie below the thermal expansion curve of reference WC, which means that WC is in compression at room temperature.

Residual strains along WC principal lattice axis are shown in Fig. 4. The average error in strain measurement is estimated at $\pm 50 \times 10^{-6}$. On cooling, compressive strains start to build-up below 800 °C and increase when temperature is decreased. Strain anisotropy is observed between the two principal directions of the hexagonal WC crystal structure, *a* and *c*. The residual strain changes as a function of temperature have been modeled by the Eshelby method [15] applied to a Co inclusion within an anisotropic WC matrix [16] as detailed in Appendix A. The model reproduces the measured strain anisotropy between the principal directions of WC. However, a relatively important deviation from the model is observed below 400 °C in particular along the c axis. The validity of the model is therefore discussed in § 4. Stresses in the WC phase are calculated according to Eq. (2) and reported in Fig. 5. Also in this case, the stresses calculated by the Eshelby method are reported on the same figure. We notice that stresses are not anisotropic like the strains. This effect could be expected by the use of the Reuss approximation. However, isotropic stresses are also predicted by the Eshelby model which does not imply such hypothesis.

The temperature dependence of the cobalt lattice parameters is presented in Fig. 6. The cobalt bulk reference was measured down to 500 °C where the fcc structure is still present. Values at room temperature are extrapolated according to thermal expansion measured in fcc powder by [17]. In WC–Co, a clear deviation from pure cobalt thermal expansion can be observed when cooling to room temperature and when heating above 800 °C. Fig. 7 reports calculated strains in cobalt with respect to the measured reference. They are the result of the mechanical effect (thermal strain) and of chemical effects as pointed out in Eq. (4). Supposing that the thermal strain should become zero at a certain temperature i.e. $\varepsilon_{Co,mech} = 0$, the additional effect and particularly the increase of Co strain above 800 °C should be attributed to the chemical effect $\varepsilon_{Co,chem}$. Therefore, cobalt strains calculated from the stress equilibrium Eq. (5) and assuming elastic isotropy are also shown in Fig. 7. They are shifted to reach the estimated threshold of $\varepsilon_{Co,chem}$ at 800 °C.

Table 1
Polynomial coefficients for the WC powder lattice parameters derived from the curves in Fig. 3 as $f(T) = \alpha + \beta T + \gamma T^2$.

	α	β	γ
a [nm]	0.29146 ± 0.00001	$(1.3218 \pm 0.03)10^{-6}$	$(1.924 \pm 0.2)10^{-10}$
c [nm]	0.28453 ± 0.00001	$(1.1698 \pm 0.02)10^{-6}$	$(1.5037 \pm 0.2)10^{-10}$

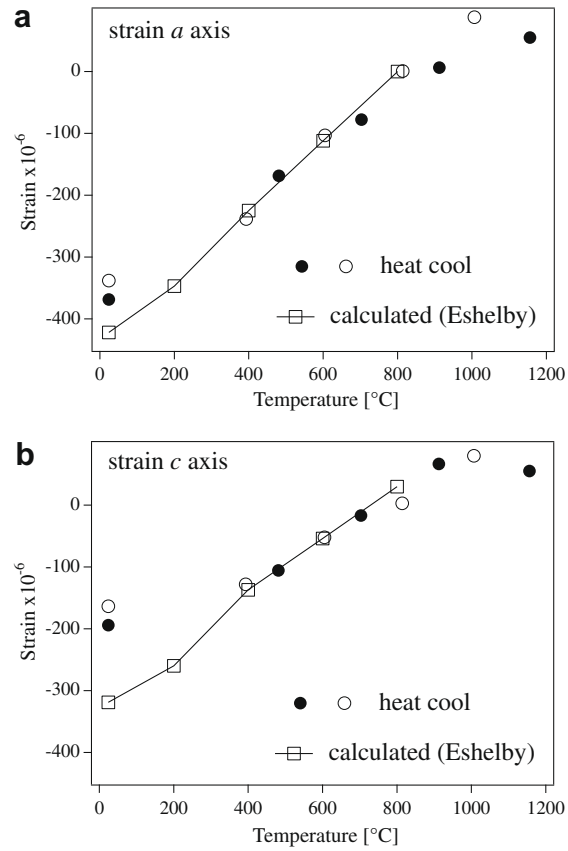

Fig. 4. Strains in WC measured as a function of temperature upon heating and cooling. Figures (a) and (b) refer to *a* and *c* hexagonal axis respectively. The data correspond to the second thermal cycle. Anisotropic strains calculated using the Eshelby model are reported on the same figure and are discussed later.

4. Discussion

4.1. WC phase

Residual thermal stresses in the WC-17.8vol.%Co are assessed upon heating from room temperature to 1156 °C in both WC and Co phases. At room temperature, the stresses in the WC are compressive as expected and reach about −400 MPa. These values are close to those measured by Refs. [4–6] for samples with a similar cobalt content. At high temperature, the stress/strain values become slightly positive but, taking into account the experimental error, they should be considered as close to zero. Therefore, we consider that residual stresses start to build-up upon cooling below the temperature of 800 °C according to the curves shown in Figs. 4 and 5. The Eshelby model we use is purely elastic even if non linear since it takes into account the variations of thermal expansion and of elastic constants with the temperature. In terms of strain, we notice an evident deviation from the model approaching room temperature, in particular along the hexagonal *c* axis. Strain anisotropy in WC is expected from both anisotropy of elastic constants and of thermal expansion. Sayers first applied [18] an

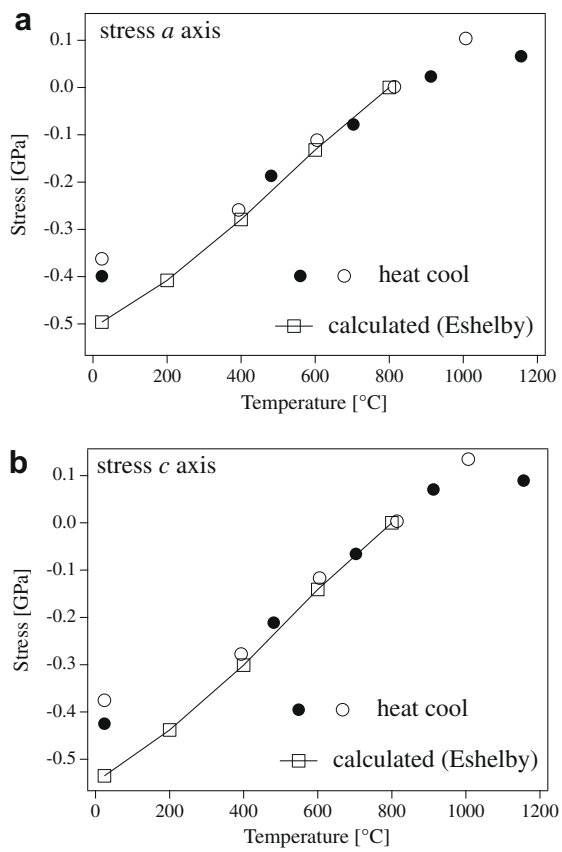

Fig. 5. Stress in WC calculated from strains (see Eq. (2)). Figures (a) and (b) refer to *a* and *c* hexagonal axis respectively. Anisotropic stresses calculated using the Eshelby model are reported on the same figure and are discussed in § 4.

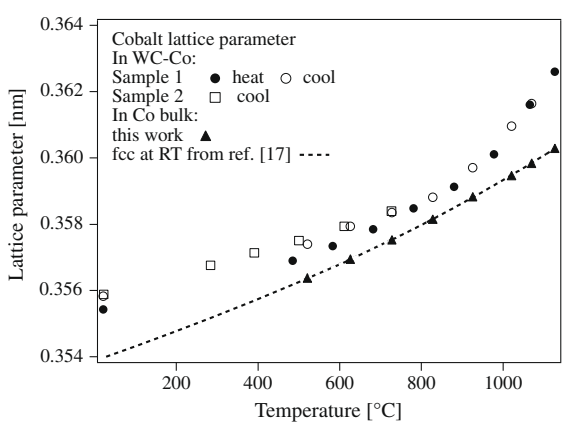

Fig. 6. Temperature dependence of cobalt lattice parameters measured in WC–Co upon heating and cooling. Low temperature measurements were obtained in a second sample. Thermal expansion of pure Co is measured in bulk cobalt above 500 °C. Low temperature values are obtained from Ref. [17].

analytical model developed for composites by Hashin [19] to the calculation of thermal stresses on an anisotropic WC sphere surrounded by a WC–Co matrix. This model predicts anisotropic compressive strains that are larger along the WC *c* axis. While developing our model we have compared it to Sayers' predictions with good agreement (see Appendix A). However, the anisotropy of WC strains obtained in this study does not correspond to Sayers' calculations. In testing different geometries for the Eshelby model, the best agreement with experimental data was found using a

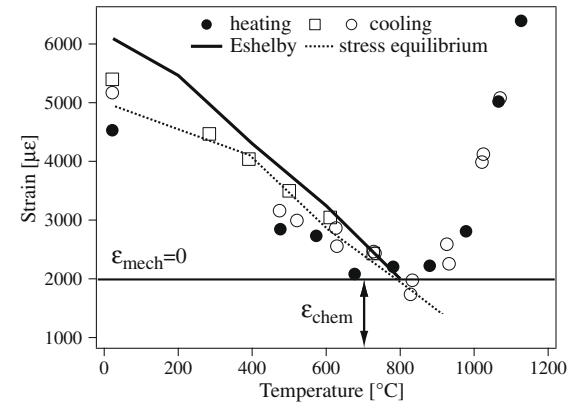

Fig. 7. Strain in cobalt calculated from comparison with pure cobalt reference (data illustrated in Fig. 6). The calculated values from stress equilibrium (Eq. (3)) and from Eshelby model are reported. Calculated values are shifted to 2000 μstrains at 800 °C.

spherical cobalt inclusion inside an anisotropic WC matrix, which corresponds with curves reported in Figs. 3 and 4. However, strains measured along the *c* axis are even lower than predicted by the present model. A possible explanation for this discrepancy may be found in considering the grain shape. It is well known that the WC grains grow anisotropically, which produces flat triangular prisms with a base (corresponding to the hexagonal (0 0 1) planes) larger than the height [20]. Seol et al. [21] demonstrated that such grain shape anisotropy should produce larger strains along the *a* axis growing with the increase of particle aspect ratio, which was found in samples analysed by neutron diffraction. On the other hand, for a WC sphere (aspect ratio=1) with anisotropic elastic constants, strains should be larger along the *c* axis in agreement with Sayers. However, since in this study, measurements were made as a function of temperature, it should be noticed that the deviation from the Eshelby model curve shown in Fig. 3 mainly occurs at low temperature. Therefore, this effect cannot just be related to the elastic distribution of stresses around the WC particles. Instead, it may be related to cobalt plasticity that locally relaxes the stresses anisotropically owing to WC grain shape. Such possibility of stress relaxation is discussed in the next paragraph.

4.2. Cobalt phase

The absolute value of strains and stresses in the Co phase cannot be derived directly from present experiments because of the lack of an appropriate reference with the same alloy composition (which is expected to vary with temperature according to the equilibrium between the WC and Co phases). On the other hand, they should comply with the stress equilibrium (Eq. (5)). Since measurements in the WC phase show that thermal stresses should be relaxed at 800 °C, the thermal stresses (strains) in the cobalt should also become zero at such temperature. The residual strain increase above 800 °C should have another origin such as WC solution into cobalt. Nishiyama and Ishida [11] produced the first measurements of the lattice parameter expansion due to W and C solution into cobalt. However, only WC was used to prepare the alloys, not enabling to separate the effect of W from that of C. They obtain a linear dependence of Co lattice expansion on W content (measured) that we have calculated to be 2700 μstrain/at.%W. In the work of Roebuck et al. [12] different Co–W–C alloys were used and the Co lattice parameter expansion Δa is given by the formula:

$$\Delta a = 3.6 \times 10^{-3} X_W + 12 \times 10^{-3} X_C \ [\mathrm{nm}]$$

where X_W, X_C are the content of tungsten, respectively carbon in atomic%. One can notice that the effect of carbon is larger than that

of W. Supposing a stoichiometric W-C solution, we have calculated a lattice expansion of 4400 μstrain/at.%W. Finally, the work of Maritzen et al. [13] also take into account the effect of mixing so that the lattice expansion is given by:

$$\Delta a = 3.69 \cdot 10^{-3} X_W + 7.63 \cdot 10^{-3} X_C - 1.08 \cdot 10^{-3} \frac{X_W X_C}{X_W + X_C} \text{ [nm]}$$

The effect of carbon seems smaller with respect to the Roebuck work but still important. Our calculation for stoichiometric W-C solution yields a lattice expansion of 3040 μstrain/at.%W.

As indicated in Fig. 7, we have shifted both the stress equilibrium curve and the values obtained from the Eshelby model by 2000 μstrains at 800 °C supposing this to be the average chemical lattice expansion of Co $\varepsilon_{Co,chem}$ at such temperature. Considering the data by Ref. [13] that seem the most accurate, the cobalt binder should contain 0.66 at.%W at 800 °C. This value should not change much even below 800 °C because of the decrease of W diffusion. In order to verify the validity of this result, we have measured the saturation magnetization at 27 °C and a value of 193.78 $\mu Tm^3/Kg$ was found. According to data provided by [13], this value should correspond to 0.68at%W stoichiometric with C, which is very close to the W content that corresponds to 2000 μstrain. Supposing that above 800 °C the cobalt lattice expansion is mainly due to WC solution, we can estimate that cobalt should contain 2.1 at.%W at 1127 °C, which is the maximum temperature attained for cobalt measurements (end of curve in Fig. 7). Effectively, thermodynamical simulation made with thermo-Calc [22] do show that a sudden increase of solubility of W is expected in WC–Co alloys between 850 °C and 950 °C [23]. The Co lattice expansion does not generate tensile stress on the WC skeleton as it might be expected. As demonstrated in [4], the cobalt expansion is compensated by the volume loss of WC at interfaces. However, in that work a model was developed to show that such volume loss was even higher than cobalt expansion and that compressive stresses in WC could develop again at high temperature. The present measurements do not support such hypothesis showing that little thermal stresses are present in WC–Co above 800 °C. We should also notice that the cobalt Curie point should be well below the maximum temperature achieved in present experiments. In fact, the highest Curie point is expected for pure cobalt at 1120 °C [11]. Even if strain effects may be expected from the magnetic transition, no abrupt change in the expansion curve is observed excluding an influence on residual stresses.

Below 800 °C, the measured cobalt strains match quite well with those calculated from stress equilibrium. They reach about 5000 μstrain at room temperature, which considering the offset of 2000 μstrain due to chemical strain, corresponds to a stress level of 1850 MPa. However, as already noticed for WC data (Figs. 3 and 4), the strains predicted by the Eshelby model deviate above those found experimentally at room temperature. This effect might be attributed to plasticity in the cobalt relaxing thermal stresses when they overcome its yield stress at low temperature. Effectively, it was shown [6] that at room temperature the cobalt thermal stresses are very close to yield that may reach 2000 MPa. Such value could appear anomalously high. In reality, the peculiar structure of the cobalt with dislocations entangled by stacking faults and its constrained state can determine very high yield stress for cobalt in WC–Co as predicted by [24]. On the other hand, the deviation we observe from the elastic behaviour is reversible, which is not compatible with classical plasticity e.g. by dislocation movement. A possible explanation could be given considering the particular microstructure of the cobalt, which is characterized by a stacking fault network [25]. These stacking faults can be considered as hcp layers in the metastable fcc structure of the cobalt. The martensitic nature of such stacking faults may cause pseudoelasticity as in thermoelastic shape memory alloys [26]. In fact, reversible shrinking of stacking faults in cobalt has been observed by "in situ" TEM [27] when thermal cycles are applied to WC–Co. In this case, some cobalt regions may be able to relax the thermal stresses that lie above a threshold. When temperature increases and the level of thermal stress decreases, the material returns to its original condition. It is the reversible movement of partial dislocations bordering stacking faults in the cobalt that may be at the origin of reversible stress relaxation. However, plastic shear strain due to dislocations should not relax hydrostatic internal stress. In the present case, the relaxation is possible because of the 3-dimensional distribution of stresses. Plasticity enables a redistribution of residual strain in the cobalt and therefore a shift of the average strain, which is measured by neutron diffraction.

5. Conclusions

Average internal elastic strains and stresses in the two-phases of a WC-17.8vol.%Co cermet were determined using the SMARTS diffractometer at the Los Alamos Neutron Science Center. This study leads to the following conclusions:

1. A particular setup was built to enable the measurement of lattice parameter of WC–Co and of reference WC and Co on the same moving frame. The thermal expansion of the two-phases has been determined up to 1156 °C.
2. The development of residual thermal mismatch stresses starts at about 800 °C. After cooling down to room temperature, the residual compressive stresses in the WC phase are ca. −400 MPa. Residual stresses are isotropic in WC. Strains instead are larger along the hexagonal *a* axis. This effect is attributed to grain shape anisotropy.
3. Residual tensile stresses in the Co phase are estimated at about 1850 MPa at room temperature in equilibrium with WC. They decrease when increasing the temperature. The lattice parameter of the cobalt is also expanded by the solution of W and C. Above 800 °C, even if thermal strains are assumed to be zero, the cobalt lattice parameter strongly increases. At room temperature, the W (and C) content should be 0.68 at.%. At 1127 °C, we can estimate that 2.1 at.%W is in solution within the cobalt. Since the data obtained are reproducible upon multiple cycles, these should be equilibrium values.
4. Residual strain changes in WC and Co were calculated using an elastically anisotropic Eshelby model. A deviation of experimental values of strain from the model is observed around room temperature. This deviation, reversible in thermal cycles, is attributed to cobalt plasticity by shrinkage (respectively expansion) of stacking faults causing a pseudoelastic behaviour.

Acknowledgments

This work has benefited from the use of the Lujan Neutron Scattering Center at LANSCE, which is funded by the Office of Basic Energy Sciences (DOE). Los Alamos National Laboratory is operated by Los Alamos National Security LLC under DOE Contract DE-AC52-06NA25396. The authors thank A.B. Sandvik Coromant for providing the samples and for financial support.

Appendix 1

The Eshelby model [15] allows for the calculation of stresses due to the difference in thermal expansion coefficients of a material inclusion within the matrix of another material. This difference leads to a misfit ε^T* between the inclusion and the corresponding matrix cavity that contains it. In this Appendix, the formulation

Table A-1
Calculated strains and stresses in the Eshelby model with different parameters. Different comparisons with the analytical model by Sayers are reported.

	Strain *a* [μstrain]	Strain *c* [μstrain]	Stress *a* [MPa]	Stress *c* [MPa]
Sayers	−290	−753	−484	−887
Present model ther.exp. by [18]	−227	−573	−374	−678
Sayers' model with present ther. exp.	−387	−423	−491	−619
Present model, WC matrix, 20vol.%Co	−365	−276	−429	−463

Table A-2
Data for the phases used in the model

Phase	f	ν	$\alpha/10^{-6}$ [K^{-1}]	E [GPa]	Temperature range [°C]
WC	0.82	0.23	5.4* *a axis* 4.8* *c axis*	700**	800-20
Co	0.18	0.32	13.8**	206**	800-20

* According to present measurement.
** Temperature variations are taken into account according to Ref. [4].

by Clyne and Withers [28] has been used. The model assumes an ellipsoidal inclusion with different elastic constants (stiffness matrix C_i) than those of the surrounding matrix (stiffness matrix C_m). In order to obtain an analytical solution, the real inclusion is replaced by an imaginary inclusion with the same elastic constants as the matrix that leads to the same final stress state. The stress state of matrix and inclusion can then be determined by the equivalent deformation ε^T of the imaginary inclusion. All deformations are assumed elastic.

The tensor of the equivalent elastic deformation ε^T of the imaginary inclusion is given as a function of the misfit ε^T* :

$$\varepsilon^T = -\{(C_m - C_i)\cdot[S - f(S-I)] - C_m\}^{-1} C_i \varepsilon^T* \quad (A.1)$$

where f is the volume fraction of the inclusions, I the identity matrix, C the stiffness tensor and S the Eshelby tensor.

From equation (A1), the average stress tensor of the matrix phase matrix $<\sigma>_m$ and the inclusion $<\sigma>_i$ can be calculated as:

$$\langle\sigma\rangle_m = -fC_m(S-I)\varepsilon^T \quad (A.2)$$

$$\langle\sigma\rangle_i = (1-f)C_m(S-I)\varepsilon^T \quad (A.3)$$

In the case, where the misfit is due to the differences in thermal expansion between matrix and inclusion, it can be expressed in terms of ε^T*:

$$(\varepsilon^T *)_j = (\alpha_i - \alpha_m)\Delta T g_j \quad (A.4)$$

where α is the thermal expansion coefficient and $g_j = 1$ for $j = 1$ to 3 and $g_j = 0$ for $j = 4$ to 6.

Our model has been first tested in comparison with the analytical model by Sayers [18]. In this model, a WC spherical particle with anisotropic elastic constants is surrounded by a WC-Co homogeneous matrix. Results of the comparison for 20vol%Co are shown in Table A-1 considering the same input parameters. The values are calculated at room temperature for a ΔT = 700 °C. When using the thermal expansion by Sayers, strain anisotropy with higher strains along the *c* axis is reproduced in out model. Another test was made by using Sayers' geometry and considering the thermal expansion coefficients measured for the WC in the present study. One can observe that the strain anisotropy has been reduced.

In the application of the model to the present measurements, it is assumed that the matrix is the WC phase (which has the larger volume fraction) and the inclusion is the Co. The parameters used in the model are given in Table A-2. A comparison with the tests of Sayers' model described above is given for a cobalt content of 20vol% in Table A-1. We notice that with our geometry the predicted strains are larger along the *a* axis.

References

[1] Gurland J. Temperature and stresses in the two-phase alloy WC–Co. Trans Amer Soc Metals 1958;50:1063–71.
[2] Öhman S, Pärnama E, Palmquist S. Studies of residual stresses in WC–Co systems. Jernkontorets Ann 1967;151:126–59.
[3] French DN. X-ray stress analysis of WC–Co cermets. J Am Ceram Soc 1969;52:267–75.
[4] Mari D, Krawitz AD, Richardson JW, Benoit W. Residual stress in WC–Co measured by neutron diffraction. Mater Sci Eng A 1996;209:197–205.
[5] Coats DL, Krawitz AD. Effect of particle size on thermal residual stress in WC–Co composites. Mater Sci Eng A 2003;359:338–42.
[6] Livescu V et al. Measurement and modeling of room temperature co-deformation in WC-10wt% Co. Mater Sci Eng A 2005;399:134–40.
[7] Clausen B, Mari D, Krawitz AD, Bourke MAM, Internal strain development during loading of cemented carbide composites. In: Bose A, Dowding RJ, editors, Proceeding of the tungsten, refractory & hardmetals VI, Orlando FL, MPIF, 460.
[8] Larson AC, Dreele RBV. General structure analysis system (GSAS). Los Alamos: Los Alamos National Laboratory; 2000.
[9] Lee M, Gilmore RS. Single crystal elastic constants of tungsten monocarbide. J Mater Sci 1982;17:2657–60.
[10] Evenschor PD, Fröhlich W, Hauk V. Calculation of X-ray elastic constants from single crystal coefficients of hexagonally crystallizing metals. Z Metallk 1971;62:38–42.
[11] Nishiyama A, Ishida R. The purity of the Cobalt phase in cemented carbides hard alloys. Trans Jpn Inst Met 1962;3:185–90.
[12] Roebuck B, Almond EA, Cottenden AM. The influence of composition, phase transformation and varying the relative F.C.C. and H.C.P. phase contents on the properties of dilute Co–W–C alloys. Mater Sci Eng 1984;66:179–94.
[13] Maritzen W, Ettmayer P, Kny E. Lattice parameters and saturation magnetization of Co–W–C alloys. Powder Metall Int 1985;17:68–71.
[14] Touloukian YS, Kirby RK, Taylor RE, Lee IR. Thermal expansion, nonmetallic solids, thermophysical properties of matter. New York: IFI/Plenum; 1977.
[15] Eshelby JD. The determination of the elastic field of an ellipsoidal inclusion, and related problems. Proc R Soc 1957;241A:76–396.
[16] Withers PJ, Stobbs WM, Pedersen OB. The application of the Eshelby method of internal stress determination to short fibre metal matrix composite. Acta Mater 1989;37:3061–84.
[17] Owen EA, Jones DM. Effect of grain size on the crystal structure of cobalt. Proc Phys Soc B 1954;67:456–66.
[18] Sayers CM. Thermal contraction stresses in cemented tungsten carbide composites. Mater Sci Eng 1987;91:195–9.
[19] Hashin Z. Thermal expansion of polycrystalline aggregates: II. Self consistent approximation. J Mech Phys Solids 1984;32:159–65.
[20] Lay S, Allibert CH, Christensen M, Wahnström G. Morphology of WC grains in WC–Co alloys. Mater Sci Eng A 2008;486:253–61.
[21] Seol K, Krawitz AD, Richardson JW, Weisbrook CM. Effects of WC size and amount on the thermal residual stress in WC–Ni composites. Mater Sci Eng A 2005;398:15–21.
[22] Sundman B, Jansson B, Andersson J-O. Termo-Calc databank system. Calphad: Comput Coupling Phase Diagrams Thermochem 1985;9:153–90.
[23] Buss K, High temperature deformation mechanisms of cemented carbides and cermets, Ph.D. Thesis no. 3095, Lausanne: EPFL; 2004.
[24] Sigl LS, Fischmeister HF. On the fracture toughness of cemented carbides. Acta Metall 1988;36:887–97.
[25] Mari D, Bolognini S, Feusier G, Viatte T, Benoit W. Experimental strategy to study the mechanical behaviour of hardmetals for cutting tools. Int J Refr Metals Hard Mater 1999;17:209–25.
[26] Funakubo H. Shape memory alloys. Gordon and Breach 1987.
[27] Schaller R, Mari D, Maamouri M, Ammann JJ. Mechanical behaviour of WC-11wt%Co studied by bending tests, internal friction and electron microscopy. J Hard Mater 1992;3:351–62.
[28] Clyne TW, Withers PJ. In: Davis EA, Ward IM, editors. An introduction to metal matrix composites. Cambridge: Cambridge University Press; 1993.